The Astrophysical Journal, 981:142 (10pp), 2025 March 10 https://doi.org/10.3847/1538-4357/adb281


# Amplifying Resonant Repulsion with Inflated Young Planets, Overlooked Inner Planets, and Nonzero Initial Δ

Yuancheng Xu[1] and Fei Dai[2]
[1] Department of Physics, Oxford University, Oxford OX1 3RH, UK; yuancheng.xu@some.ox.ac.uk
[2] Institute for Astronomy, University of Hawai'i, 2680 Woodlawn Drive, Honolulu, HI 96822, USA
*Received 2024 October 3; revised 2025 February 3; accepted 2025 February 3; published 2025 March 5*

## Abstract

Most multiplanet systems around mature (∼5 Gyr old) host stars are nonresonant. Even the near-resonant planet pairs still display 1%–2% positive deviation from perfect period commensurabilities (Δ) near first-order mean motion resonances (MMRs). Resonant repulsion due to eccentricity tides was one of the first mechanisms proposed to explain the observed positive Δ. However, the inferred rates of tidal dissipation are often implausibly rapid (with a reduced tidal quality factor $Q_p' \lesssim 10$). In this work, we attempt to amplify eccentricity tides with three previously ignored effects. (1) Planets tend to be inflated when they were younger. (2) Kepler-like planets likely form as resonant chains parked at the disk inner edge; overlooked inner planets could have contributed to tidal dissipation of the whole system. (3) Disk migration captures planets into first-order MMR with nonzero initial deviation Δ, thereby lowering the amount of dissipation needed. We show that even after accounting for all three effects, $Q_p'$ can only be amplified by about 1 order of magnitude, and still falls short of $Q_p'$ values of solar system planets. Therefore, eccentricity tides alone cannot fully explain the observed Δ distribution. Other effects such as obliquity tides, planetesimal scattering, expanding disk inner edge, disk turbulence, divergent encounters, and dynamical instabilities must have contributed to dislodging planets from first-order MMR.

*Unified Astronomy Thesaurus concepts:* Exoplanet astronomy (486); Exoplanet tides (497); Exoplanet dynamics (490)

## 1. Introduction

There is mounting evidence that most Kepler-like planets initially formed as a resonant chain (S. M. Mills et al. 2016; T. J. David et al. 2019; R. Luque et al. 2023; J. M. Wittrock et al. 2023; M. L. Wood et al. 2023; M. G. Barber et al. 2024; F. Dai et al. 2024; J. H. Hamer & K. C. Schlaufman 2024; S. Vach et al. 2024) parked at the disk inner edge (F. S. Masset et al. 2006; A. Izidoro et al. 2017; M. Ogihara et al. 2018; F. Dai et al. 2023; K. H. Wong & M. H. Lee 2024). This is before the resonant configurations are disrupted during subsequent dynamical evolution (Y. Matsumoto & M. Ogihara 2020; G. Pichierri & A. Morbidelli 2020; A. Emsenhuber et al. 2021; M. Goldberg et al. 2022; S. Wang & D. N. C. Lin 2023). Type I disk migration, a gravitational interaction between planets and the protoplanetary disk, is likely responsible for the migration toward the central star and the capture into resonant states (P. Goldreich & S. Tremaine 1979; D. N. C. Lin & J. Papaloizou 1986; W. R. Ward 1997; D. McNeil et al. 2005; C. Terquem & J. C. B. Papaloizou 2007; R. P. Nelson 2018).

Recently, F. Dai et al. (2024) showed that the resonant configuration is predominant for planetary systems less than 100 Myr old. On the other hand, mature Kepler planets (median age 4.6 Gyr old, T. A. Berger et al. 2020) are generally nonresonant (W. J. Borucki et al. 2011; D. C. Fabrycky et al. 2014). Only 15% of neighboring pairs are near first-order mean-motion resonance (MMR; S. Huang & C. W. Ormel 2022; F. Dai et al. 2024); these near-resonant pairs still show 1%–2% positive deviation from period ratios that are perfect integers. The deviation Δ, is defined as $\frac{P_{\rm out}/P_{\rm in}}{(k+1)/k} - 1$, where $P_{\rm out}$ and $P_{\rm in}$ represent the orbital periods of the outer and inner planets of a neighboring pair and $k$ is the small integer specifying the specific resonance.

Resonant repulsion, particularly that due to eccentricity tides, was one of the first proposed explanations for the observed positive Δ (J. C. B. Papaloizou & C. Terquem 2010; Y. Lithwick & Y. Wu 2012; K. Batygin & A. Morbidelli 2013; J. B. Delisle & J. Laskar 2014). If a planet is on an eccentric orbit, the planet is strongly deformed at the pericenter and less so at the apocenter. This variation in deformation as a function of orbital phase leads to tidal dissipation within the planet, thus draining orbital energy. On the other hand, a nonzero eccentricity can be maintained by the resonant interaction between the planets near MMR. In fact, Io's strong volcanism was predicted to be maintained by the competing effect of resonant interaction and tidal dissipation (S. J. Peale 1976).

While energy is dissipated, there is generally no net torque during the tidal evolution of eccentricity (C. D. Murray & S. F. Dermott 1999). Y. Lithwick & Y. Wu (2012) derived that the rate of change of Δ follows

$$\Delta^2\frac{d\Delta}{dt} \approx 0.006^3\left(\frac{Q}{10}\right)^{-1}\left(\frac{k_2}{0.1}\right)\left(\frac{M_{\rm p}}{10\,M_\oplus}\right)\left(\frac{R_{\rm p}}{2\,R_\oplus}\right)^5 \times\left(\frac{M_\star}{M_\odot}\right)^{-8}\left(\frac{P_{\rm orb}}{5\ {\rm days}}\right)^{-13/3}\left(\frac{1}{5\ {\rm Gyr}}\right) \times(2\beta+2\beta^2) \quad (1)$$

where $k_2$, $M_p$, $R_p$, and $P_{\rm orb}$ are the tidal Love number, mass, radius, and orbital period of the inner planet of a resonant pair. $\beta = \frac{M_{\rm out}\sqrt{a_{\rm out}}}{M_{\rm in}\sqrt{a_{\rm in}}}$ is the ratio of the masses and semimajor axes of the outer and inner planets engaged in resonance. The reduced tidal quality factor of the inner planet is given by $Q_p' \equiv Q/k_2$.

By integrating Equation (1), one can trace out the evolution of $\Delta$ from some initial value to a final value: $\Delta_f^3 - \Delta_i^3 = \Delta_{\rm mig}^3$. The observed $\Delta = \Delta_f$, coupled with the system's age and various planetary and stellar parameters in Equation (1), could provide a constraint on the reduced tidal quality factor $Q_p'$. Previous works (Y. Lithwick & Y. Wu 2012; M. H. Lee et al. 2013; A. Silburt & H. Rein 2015; S. Millholland & G. Laughlin 2019) pointed out that the inferred $Q_p'$ is often implausibly small ($Q_p' \lesssim 10$). In contrast, the terrestrial planets in the solar system have $Q_p' \sim 1000$ (P. Goldreich & S. Soter 1966), while the giant planets have $Q_p' \gtrsim 10^5$ (W. C. Tittemore & J. Wisdom 1990; C. D. Murray & S. F. Dermott 1999). Earth's $Q_p'$ is approximately 100 because we have a shallow ocean and thus strong dissipation due to tides breaking in coastal regions (C. F. Yoder 1995; C. D. Murray & S. F. Dermott 1999). This is unlikely to be the case for exoplanets, especially considering that mini-Neptunes are likely covered in a thick layer of volatile envelopes (e.g., Y. Wu 2005).

In this study, we make one more attempt to salvage the resonant repulsion due to eccentricity tides. We explore three previously ignored effects:

1. When planets were younger, they had inflated radii (e.g., J. J. Fortney et al. 2007). As shown in Equation (1), the instantaneous rate of change $\Delta$ varies as the fifth power of the planetary radius. A young, inflated planet should have experienced stronger eccentricity tides.
2. Kepler-like planets likely formed initially as a chain of resonances parked at the disk inner edge (A. Izidoro et al. 2017; F. Dai et al. 2024; K. H. Wong & M. H. Lee 2024). Moreover, for a chain of resonant planets, the tidal dissipation on the innermost planet could induce resonant repulsion on all planets involved in the resonant chain (J. C. B. Papaloizou et al. 2017; R. Brasser et al. 2022; F. Dai et al. 2023). An overlooked inner planet could produce stronger resonant repulsion than what is inferred based on the longer-period planets in the same system.
3. During disk migration, planets are captured into resonance with a nonzero $\Delta$ (deviation from perfect period ratio) to begin with (see, e.g., N. Choksi & E. Chiang 2020; F. Dai et al. 2023). The initial $\Delta_i$ depends on the ratio between semimajor axes and eccentricity damping timescales. Previous investigations on resonant repulsion have assumed $\Delta_i = 0$. This would again overestimate the amount of tidal dissipation needed to reproduce the observed $\Delta_f$.

In this study, we carefully examine all three effects and determine whether they can significantly lower the tidal dissipation rate (equivalent to increasing $Q_p'$) required to reproduce the observed $\Delta$ distribution. We try to reconcile the $Q_p'$ based on the observed near-resonant exoplanets and $Q_p'$ inferred for solar system planets. In Section 2, we describe the sample used in this study. In Section 3, we describe each of the three effects and their influences on $Q_p'$. We summarize and discuss our findings in Section 4.

## 2. Sample Selection

We start with the confirmed planet sample from the NASA Exoplanet Archive[3] retrieved on 2024 August 15. We focused on the transiting planets from the Kepler sample for two reasons: (1) orbital periods are much better measured in transit surveys than by other methods; (2) we could constrain the ages of the systems by cross-matching with the isochronal ages from T. A. Berger et al. (2020). For planets without reported masses, we predict the mass using the observed radius and the mass–radius relationship of J. F. Otegi et al. (2020).

The distribution of period ratios of our sample is similar to that in previous works (D. C. Fabrycky et al. 2014; S. Huang & C. W. Ormel 2022; F. Dai et al. 2024). Namely, $\Delta$ shows a preference for positive deviation at a level of a few percent (see also E. Louden et al. 2023). We identified the near-resonant neighboring pairs as those with $\Delta$ values within 0%–3% of each first-order period commensurability (2:1, 3:2, 4:3, 5:4, and 6:5), resulting in approximately 110 pairs within this range. The choice of 3% is based on the suggestions by previous works such as S. Huang & C. W. Ormel (2022) and F. Dai et al. (2024). Both works reported that about 15% of neighboring pairs of confirmed planets have period ratios below this threshold. Since we are interested in the tidal dissipation of Kepler-like planets, we removed giant planets ($>10\ R_\oplus$). We have also removed planets whose orbital periods imply they are too far away to have been affected by tides ($P_{\rm orb} > 30$ days). We have tested that the locations of the radius and period cuts do not change the qualitative result of this paper. These cuts resulted in 80 pairs of near-resonant planets in our sample (see Table 1 in the Appendix).

## 3. Methods and Results

The key analysis in this paper is as follows. For each observed near-resonant pairs of planets (Table 1 in the Appendix), we numerically integrated Equation (1) using the observed system parameters, and the isochronal ages from T. A. Berger et al. (2020). We can thus turn the observed deviation in period ratio $\Delta$ into a constraint on the tidal dissipation rate $Q_p'$. We then repeated the analysis incorporating sequentially the effects of inflated planet radii, overlooked inner planets, and nonzero initial $\Delta_i$, and observed how the inference on $Q_p'$ is affected. Because there are substantial uncertainties on a number of system parameters, notably the masses of the planets, the age of the system, and other parameters that will be described shortly, we performed a bootstrap analysis by resampling 100 times with measurement uncertainties for each resonant pair in our sample.

### 3.1. Radius Inflation

Young planets with a gaseous envelope cool and contract as they age (e.g., J. J. Fortney et al. 2007). Early on in a system's history, the mini-Neptunes ($>2\ R_\oplus$), i.e., those with H/He envelopes, should be inflated. Indeed, the majority of young planets discovered so far have significantly larger radii than mature planets. Many young planets have radii between 4 and 10 $R_\oplus$ (e.g., T. J. David et al. 2019; P. Plavchan et al. 2020; A. W. Mann et al. 2022; S. Vach et al. 2024) i.e., substantially larger than the mature mini-Neptunes (whose occurrence drops off quickly beyond 3.5 $R_\oplus$; B. J. Fulton et al. 2017). Although most super-Earths ($<2\ R_\oplus$) are currently exposed rocky cores (C. D. Dressing et al. 2015; L. A. Rogers 2015; F. Dai et al. 2019) or enshrouded in atmospheres of large mean molecular weight (R. Hu et al. 2024), early on they could have a primordial H/He envelope that was subsequently lost due to

[3] https://exoplanetarchive.ipac.caltech.edu (NASA Exoplanet Science Institute 2020).

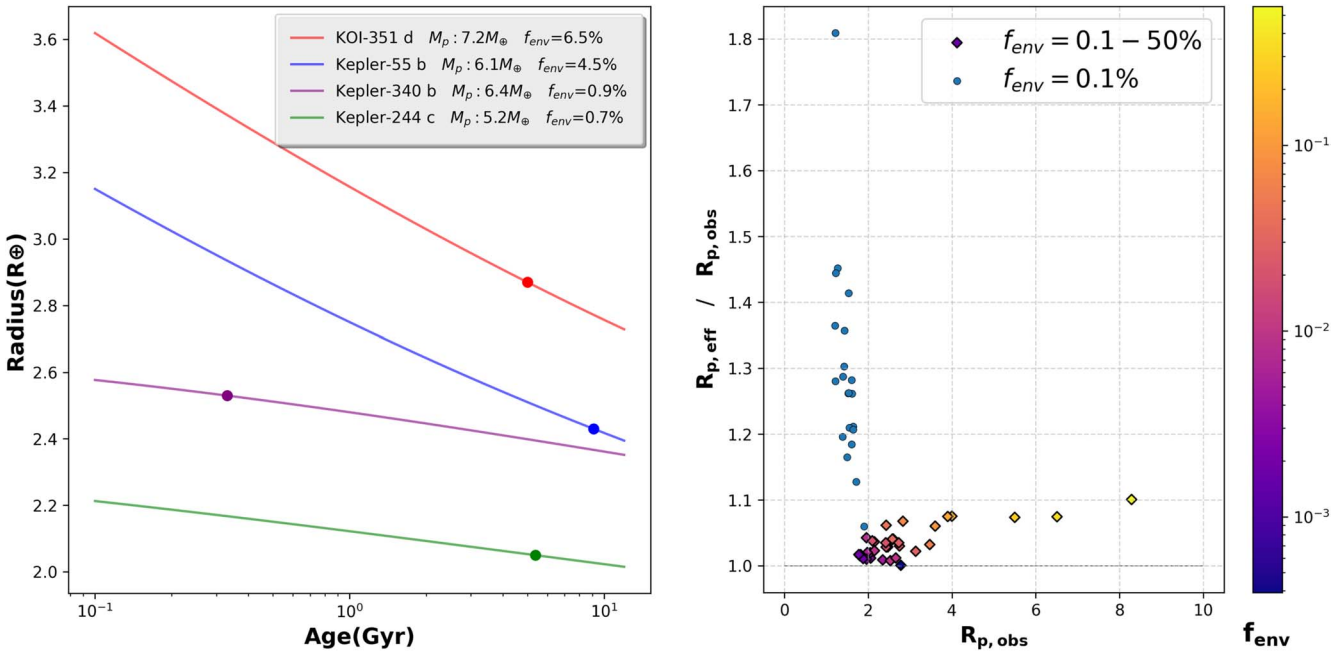


**Figure 1.** Left: the radius evolution of a few planets in our sample according to fitting shown in Table 4 (valid from 0.1 to 10 Gyr) of H. Chen & L. A. Rogers (2016) for a wide range of envelope mass fraction $f_{env}$. The circles are the current radii of the planets. Right: the effective radii vs. the current radii of the planets in our sample. The effective radius is a constant radius that should be used in Equation (1) to account for the effect of radius evolution. Super-Earths (blue points) were assumed to have an initial H/He envelope of $f_{env} = 0.1\%$. Mini-Neptunes have $f_{env} = 0.1\%$–50% and were solved using their current masses and radii.

atmospheric erosion (J. E. Owen & Y. Wu 2017; S. Ginzburg et al. 2018).

In either case, Equation (1) should account for the inflated radii of young planets. The influence of radius evolution could be substantial since the instantaneous rate of change $\Delta$ varies as the fifth power of the planetary radius. We adopt the radius evolution model of H. Chen & L. A. Rogers (2016), which is based on Modified Experiments in Stellar Astrophysics simulations (B. Paxton et al. 2015).

The model by H. Chen & L. A. Rogers (2016) accounts for the core luminosity, heavy elements, atmospheric boundary condition, and hydrodynamic atmospheric erosion, all of which are relevant effects for the radius evolution of a planet with an H/He envelope. Using the age, the planet mass, and insolation, we solved for the current mass fraction of the H/He envelope $f_{env}$ on the planets in our sample using H. Chen & L. A. Rogers (2016). This results in $f_{env}$ between ~0.1% and ~10% for the mini-Neptunes ($>2\ R_\oplus$) in our sample (see also Table 1 ). For the super-Earths within our sample ($<2\ R_\oplus$), H. Chen & L. A. Rogers (2016) usually predict a vanishingly low present-day $f_{env} < 10^{-5}$. We adopted a simple prescription that planets with radii between 1.2 and 2 $R_\oplus$ have an initial $f_{env} = 0.1\%$ whereas planets with radii $<1.2\ R_\oplus$ have no primordial H/He envelope. This choice is motivated by both theoretical studies of gas accretion onto planets of different core masses (e.g., E. J. Lee 2019) and observational work that revealed bare rocky surfaces on terrestrial-sized planets (e.g., L. Kreidberg et al. 2019; I. J. M. Crossfield et al. 2022; M. Zhang et al. 2024).

The left panel of Figure 1 shows the radius evolution up to 10 Gyr old. We show a representative set of four planets that have present-day $f_{env}$ between 0.2% and 25%. We plugged the radius evolution into Equation (1) to determine how much effect it has on the inferred tidal dissipation rate $Q_p'$. To facilitate our discussion, we defined an effective radius, which is basically a constant radius that would produce the same amount of resonant repulsion as if the full radius evolution had been included. This effective radius is simply the time average of the fifth power of the radius, $\int_0^{t_{age}} R(t)^5 dt = R_{eff}^5 \times t_{age}$.

Using the radius evolution from H. Chen & L. A. Rogers (2016), we found that the effective radius $R_{eff}$ is only of order 5% ± 3% larger than the current radius for the mini-Neptunes ($>2\ R_\oplus$); see Figure 1, right panel. The effect is stronger for the super-Earths ($<2\ R_\oplus$), and the effective radius $R_{eff}$ is about 26% ± 15% larger than the current radius. This is likely because the lower surface gravity on super-Earths cannot hold on to the atmospheres as well. For terrestrial-sized planets ($<1.2\ R_\oplus$), there is no effect of radius inflation because we assumed no primordial envelopes.

The effect of radius inflation increased the reduced tidal quality factor $\log(Q_p')$ by 0.11 ± 0.08 for mini-Neptunes ($>2\ R_\oplus$) or by 0.5 ± 0.2 for super-Earths ($<2\ R_\oplus$) as shown in Figure 2. In other words, the effect is roughly half an order of magnitude.

### 3.2. Overlooked Inner Planets

Kepler-like planets might have formed initially in a chain of MMRs (A. Izidoro et al. 2017; F. Dai et al. 2024) parked at the inner disk edge (F. S. Masset et al. 2006; K. H. Wong & M. H. Lee 2024). In addition, it has been shown both theoretically and by direct *N*-body simulations that the tidal dissipation on one planet could induce resonant repulsion on all other planets involved in a resonant chain (J. C. B. Papaloizou et al. 2017; R. Brasser et al. 2022; F. Dai et al. 2023). This is because the resonant interaction can transmit the effect of tidal dissipation from one planet to its resonant neighbors.

This is particularly important for systems that have planets closer to the host star than the resonant pairs of planets under investigation. These inner planets could include a planet that

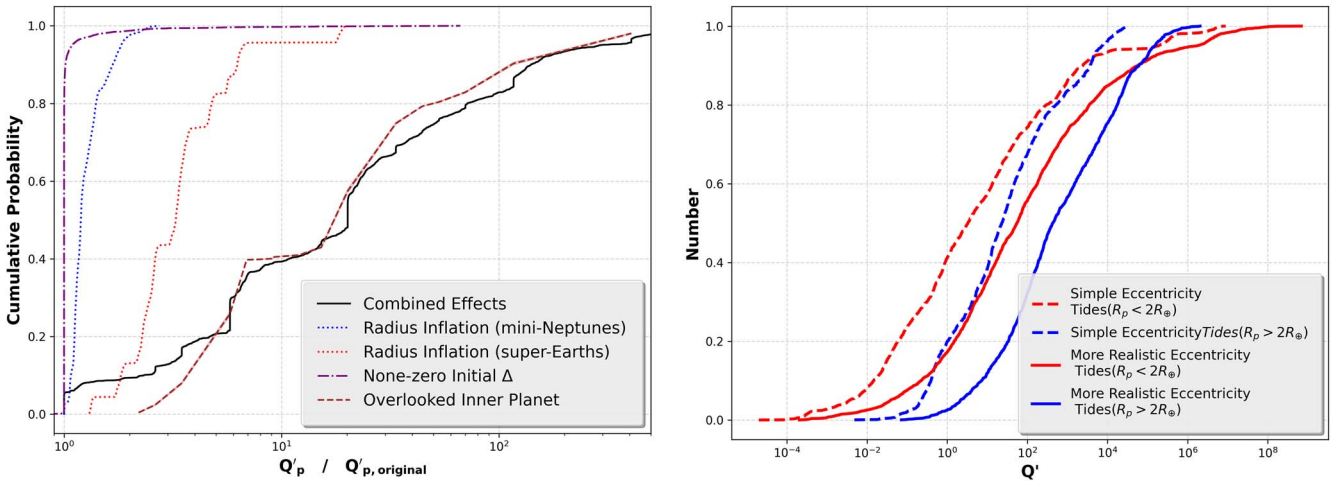


**Figure 2.** Left: the change in the reduced tidal quality factor after accounting for radius evolution (dotted line), overlooked inner planets (dashed line), and nonzero initial $\Delta$ (dashed–dotted line). The combined effect is shown by the black solid line. Radius evolution could increase $\log_{10} Q_p'$ by $0.11 \pm 0.08$ for mini-Neptunes ($>2\ R_\oplus$) or $0.5 \pm 0.2$ for super-Earths ($<2\ R_\oplus$). An overlooked inner planet can increase $\log_{10} Q_p'$ by $1.0 \pm 0.4$. Nonzero initial $\Delta$ only increases $\log_{10} Q_p'$ by $<0.1$ in 95% of cases. The combined effect may change $Q_p'$ by one order of magnitude or so. Right: $Q_p'$ as inferred in a simple eccentricity tide model vs. that after accounting for radius inflation, overlooked inner planets, and nonzero initial $\Delta$. Using a simple eccentricity tide model, the tidal quality factor required to reproduce observed planetary systems is $\log_{10}(Q_p') = 0.1 \pm 2.1$ for super-Earths (red dotted line) and $\log_{10}(Q_p') = 1.5 \pm 1.6$ for mini-Neptunes ($>2\ R_\oplus$) (blue dotted line). After accounting for the three effects mentioned above, $Q_p'$ increased by about one order of magnitude: $\log_{10}(Q_p') = 1.2 \pm 2.1$ for the super-Earths and $\log_{10}(Q_p') = 2.4 \pm 1.7$ for mini-Neptunes. These values are still too small compared to solar system values ($10^3$ for terrestrial planets and $10^5$ for the icy giants).

has not been detected yet in a transit survey, or a planet that is detected in transit but is no longer near resonance due extended resonant repulsion. In Figure 3, we show the observed orbital architectures of Kepler-80 (M. G. MacDonald et al. 2016), Kepler-176 (J. F. Rowe et al. 2014), Kepler-197 (S. Hadden & Y. Lithwick 2014), Kepler-24 (E. B. Ford et al. 2012), and K2-268 (J. H. Livingston et al. 2018). In each of these cases, the innermost planet is currently far from MMR, but could have started as part of the resonant chain and contributed significantly to resonant repulsion before dislodging itself from the resonant chain.

We performed the following analysis to quantify how an overlooked inner planet would change our inference on the tidal dissipation rate $Q_p'$. We assumed that all resonant systems were parked by inner disk edges (F. S. Masset et al. 2006; K. H. Wong & M. H. Lee 2024). Thus, we expect the orbital period of the innermost planet should follow the distribution of the inner disk edge. Adopting the magnetospheric truncation picture (S. L. Shapiro & S. A. Teukolsky 1986; K. Batygin et al. 2023), the distribution of rotation periods of young stars (e.g., in Rho Ophiuchus, $\sim$1 Myr old, which is still in the disk-hosting stage; L. M. Rebull et al. 2018) should be a good proxy for the distribution of orbital periods of the innermost planets of a resonant chain system.

For planetary systems whose innermost planets were on orbits longer than 20 days, we introduced additional inner planets. We chose a threshold of 20 days because 99% of young stars in Rho Ophiuchus have a rotation period shorter than this (Figure 4). Therefore, 20 days serves as a conservative estimate for the upper limit of the disk's inner edge, which in turn determines the orbital periods of the innermost planets in multiplanet systems parked at the disk's inner edge.

The additional planets introduced were assigned the same mass, radius, and envelope fraction as the observed innermost planet. Their orbital periods were drawn randomly, assuming they were in first-order MMR (2:1, 3:2 etc) with planets of longer periods. We added up to two additional planets if the orbital period of the first planet added is still beyond 20 days. Since tidal effects are stronger for planets with smaller semimajor axes, we calculated the tidal dissipation rate $Q_p'$ on the overlooked planets. We found that an overlooked inner planet could increase $\log(Q_p')$ by $0.9 \pm 0.3$, i.e., almost 1 order of magnitude.

We note that the additional planets introduced here could easily evade transit detection if they have a moderate mutual inclination relative to other planets in the system. For instance, a planet orbiting a Sun-like star on a 10 day orbit would enter a nontransiting configuration with an orbital inclination of 87°. A 3° mutual inclination is very typical for Kepler-like systems according to previous population-level analysis of transit multiplicity and transit durations (J. Fang & J.-L. Margot 2012; D. C. Fabrycky et al. 2014). Furthermore, observational evidence indicates that the innermost planet in multiplanet systems often exhibits the largest mutual inclination (F. Dai et al. 2018). For example, the innermost planet of K2-266 has a mutual inclination $>10°$ (J. E. Rodriguez et al. 2018). The innermost planet Kepler-176 b has a $>3.^\circ5$ mutual inclination relative to its resonant neighboring planets (J. F. Rowe et al. 2014; see also Figure 3). Mercury, the innermost planet in the solar system, is the most inclined (7° tilt from the ecliptic; C. D. Murray & S. F. Dermott 1999). This phenomenon can be attributed to secular interactions between planets, which redistribute the angular momentum deficit (Y. Lithwick & Y. Wu 2011). The innermost planet has the lowest angular momentum deficit per unit mass. Given some angular momentum deficit, the innermost planet can be readily excited into an inclined orbit. In the case of the innermost planet in a resonant chain, once it dislodges from MMR, its orbital inclination may evolve further due to secular effects or coupling with the stellar quadrupole (C. Spalding & K. Batygin 2016). The enhanced mutual inclination on the innermost planets makes them less likely to be detected by transit surveys such as Kepler (W. J. Borucki et al. 2011) and TESS (G. R. Ricker et al. 2014).

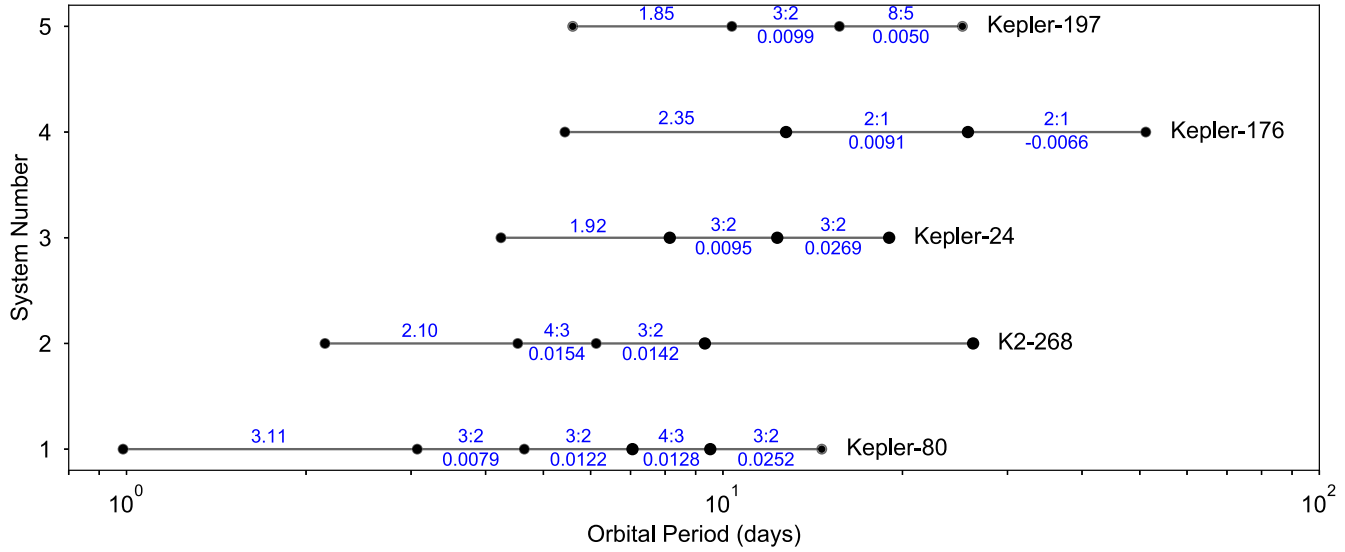


**Figure 3.** The orbital architecture of representative near-resonant multiplanet systems where the innermost planets are currently far away from MMR. However, the innermost planets could have been part of the resonant chain initially and contributed to the resonant repulsion of the whole system. Near-resonant pairs are labeled in blue using both the MMR and the observed $\Delta$.

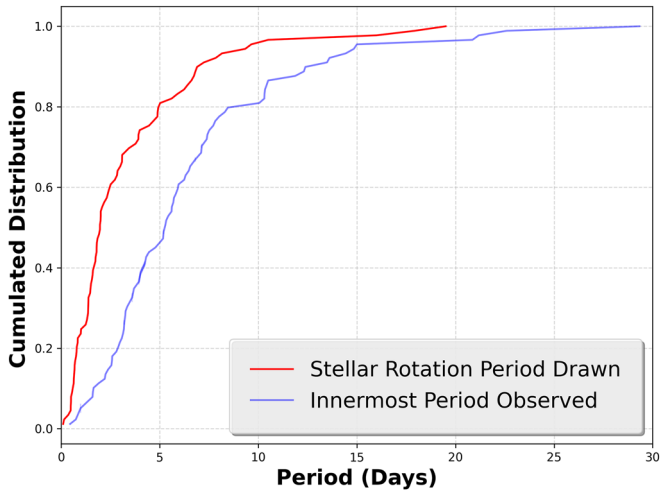


**Figure 4.** The orbital periods of inner planets of the whole system and distribution of stellar rotation periods of rho Ophiuchus (L. M. Rebull et al. 2018), which serves a proxy for the orbital period of an overlooked inner planet.

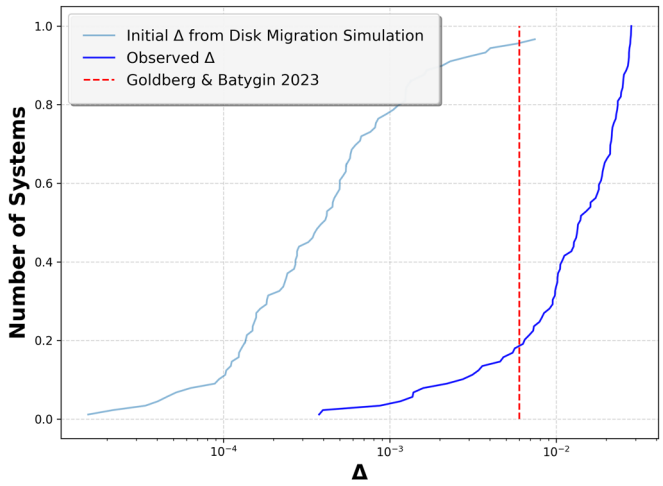


**Figure 5.** The distribution of $\Delta_i$ ($\log_{10}(\Delta_i) = -3.4 \pm 0.5$) from our disk migration simulations (F. Keller & F. Dai 2025, in preparation) and the observed $\Delta$ ($\log_{10}(\Delta) = -1.9 \pm 0.4$) on near-resonant planets. M. Goldberg & K. Batygin (2023) proposed an empirical boundary for separating the librating vs. circulating planets at $\Delta = 0.6\%$ or $\log_{10}(\Delta) = -2.2$ (red dashed line). Most observed multiplanet systems are near resonance (circulating) rather in resonance (librating). Conversely, most planetary systems produced by convergent disk migration are in resonance (librating).

Once the innermost planet breaks away from MMR, secular interactions dominate over resonant effects and can continue to increase the orbital eccentricity of these planets (K. C. Schlaufman 2010; C. Petrovich et al. 2019; B. Pu & D. Lai 2019). Consequently, tidal forces may remain active, gradually shrinking the planets' orbits. Eventually, the orbital periods between those of the innermost planets and longer-period companions may may deviate significantly from the initial MMR configuration. This scenario may explain the systems in Figure 3. Furthermore, once the innermost planets lose the stabilizing influence of MMR, orbital instability may quickly follow. Dynamical simulations by R. Li et al. (2024) demonstrated that merger events can effectively randomize the period ratios of colliding planets, thereby erasing any trace of the MMR the system may have initially exhibited. Additionally, mutual inclinations generated during close encounters could render the planets nontransiting (or "missing") as discussed earlier in this section.

### 3.3. Nonzero Initial $\Delta$

Many disk migration simulations have demonstrated that when planets are captured into first-order MMR during migration, they will end up at a range of initial deviations in period ratio $\Delta$ (e.g., G. Pichierri et al. 2018; N. Choksi & E. Chiang 2020; F. Dai et al. 2023).

During disk migration, the orbital eccentricity $e$ is damped down by the gaseous disk while it is also pumped up by resonant interaction between the planets. The equilibrium eccentricity is determined by the balance of the pumping and damping of $e$ (C. Terquem & J. C. B. Papaloizou 2019).

In short, depending on the amount of eccentricity damping in the disk, resonant planets may have a range of initial $e$ and hence a range of nonzero $\Delta$. In a companion paper (F. Keller & F. Dai 2025, in preparation), we carried out thousands of

convergent disk migrations with a wide range of planetary and disk parameters including different $e$ damping timescales. We found that for planets that engaged into librating first-order MMR during disk migration, their initial $\Delta$ has a log-normal distribution with a mean at $\log_{10}(\Delta) = -3.4 \pm 0.5$ (Figure 5).

On the other hand, the observed near-resonant planets in our sample have $\log_{10}(\Delta) = -1.9 \pm 0.4$, i.e., the classical 1%–2% deviation from a perfect integer ratio (D. C. Fabrycky et al. 2014). We compare and contrast the $\Delta$ distribution from disk migration simulations and the observed systems in Figure 5. M. Goldberg & K. Batygin (2023) proposed that the empirical boundary for separating the librating versus circulating planets is at $\Delta = 0.6\%$ or $\log_{10}(\Delta) = -2.2$. Most observed near-resonant planets are in a state of circulation rather than libration.

An inspection of Equation (1) shows that the amount of tidal dissipation $Q'_p$ is proportional to $(\Delta_f^3 - \Delta_i^3)^{-1}$. In other words, a nonzero $\Delta_i$ would lower the amount of tidal dissipation required to explain the observed $\Delta_f$ distribution. For each near-resonant planet pair in our sample, we bootstrapped 100 times, each time drawing a random $\Delta_i$ from our disk migration simulations along with other uncertainties such as planet mass and system age. We numerically integrated Equation (1) to determine the change of $Q'_p$.

The initial and observed $\Delta$ distributions differ by roughly 1.5 orders of magnitude ($\log_{10}(\Delta_f) = -3.4 \pm 0.5$ versus $\log_{10}(\Delta_f) = -1.9 \pm 0.4$). Moreover, $Q'_p$ is proportional to $(\Delta_f^3 - \Delta_i^3)^{-1}$; the third power further accentuates the difference between $\Delta_f$ and $\Delta_i$. Our results suggest that nonzero initial $\Delta_i$ has minimal impact on $Q'_p$. It can only increase $Q'_p$ by no more than a factor of two (Figure 2).

## 4. Discussion

### 4.1. Resonant Repulsion Is Not the Full Story

Our resonant repulsion model successfully reproduced a result from the literature (Y. Lithwick & Y. Wu 2012; M. H. Lee et al. 2013; A. Silburt & H. Rein 2015; S. Millholland & G. Laughlin 2019), namely that the traditional treatment of eccentricity tides requires extremely rapid tidal dissipation rates to explain the observed $\Delta$ distribution. Specifically, a reduced tidal quality factor of $\log_{10}(Q'_p) = 0.1 \pm 2.1$ is needed for super-Earths and terrestrial-sized planets ($<2\ R_\oplus$), and $\log_{10}(Q'_p) = 1.5 \pm 1.6$ is needed for mini-Neptunes ($>2\ R_\oplus$). These values are clearly at odds with the solar system estimates of $\log_{10}(Q'_p) = 3$ and 5 for the terrestrial planets and icy giant planets respectively (C. D. Murray & S. F. Dermott 1999). See the right panel of Figure 2.

The three additional effects investigated in this paper can moderately enhance the effect of resonant repulsion driven by eccentricity tides:

1. We found that accounting for inflated radii on young planets may increase $\log(Q'_p)$ by $0.11 \pm 0.08$ for mini-Neptunes ($>2\ R_\oplus$) or $0.5 \pm 0.2$ for super-Earths ($<2\ R_\oplus$) (Figure 2). In other words, radius inflation could increase the required tidal quality factor by half an order of magnitude.
2. By including additional planets that lie closer to the host star than the observed resonant pairs, the tidal quality factor $\log_{10} Q'_p$ can increase by $0.9 \pm 0.3$, i.e., almost an order of magnitude.
3. Disk migration deposits planets into MMR with nonzero initial $\Delta$. However, according to our disk migration simulations (F. Keller & F. Dai 2025, in preparation), the initial $\Delta_i$ are generally small, $\log_{10}(\Delta_i) = -3.4 \pm 0.5$. Including such small initial $\Delta_i$ in the evolution of resonant repulsion can only increase $\log_{10} Q'_p$ by $<0.1$ in 95% of the cases. See the left panel of Figure 2.

Our resonant repulsion model incorporates all three effects simultaneously. With these effects included, the tidal quality factor increases to $\log_{10}(Q'_p) = 1.2 \pm 2.1$ for the super-Earths and terrestrial-sized planets and to $\log_{10}(Q'_p) = 2.4 \pm 1.7$ for mini-Neptunes ($>2\ R_\oplus$). This is an improvement over previous estimates in simple models of eccentricity tidal. However, our $Q'_p$ are still discrepant from the solar system values of $\log_{10}(Q'_p) = 3$ and 5 for rocky and gaseous planets. See the right panel of Figure 2.

We further highlight that the near-resonant planetary systems HD 109833 (~20 Myr old, a member of the Lower Centaurus Crux; M. L. Wood et al. 2023) and V1298 Tau (~20 Myr old, a member of the Taurus–Auriga; T. J. David et al. 2019). These systems are so young that eccentricity tides likely have not had sufficient time to operate. Yet, the near-resonant pairs in HD 109833 and V1298 Tau (J. Livingston et al. 2025, in preparation) can have deviation $\Delta = 0.8\%$–1% from perfect integer ratios. Such significant $\Delta$ at such a young age cannot be explained by resonant repulsion driven by eccentricity tides.

Another limitation of the resonant repulsion model due to eccentricity tides is its inconsistency with observed transit timing variation (TTV) systems. Specifically, planetary systems with TTVs often exhibit nonzero TTV phases (Y. Lithwick et al. 2012; S. Hadden & Y. Lithwick 2017; N. Choksi & E. Chiang 2023; M. Goldberg & K. Batygin 2023). TTV phases are a proxy for the free eccentricities of near-resonant planets, with substantial free eccentricities generally producing measurable TTV phases. In order to generate the observed $\Delta$ of ~1% in resonant repulsion, a planetary system must evolve over tens to hundreds times the eccentricity damping timescale $\tau_e$ (Y. Lithwick & Y. Wu 2012; M. Goldberg & K. Batygin 2021). This process effectively eliminates free eccentricities, resulting in negligible TTV phases. Yet, nonzero TTV phases are commonly seen in TTV systems (N. Choksi & E. Chiang 2023; M. Goldberg & K. Batygin 2023). This discrepancy further underscores the limitations of resonant repulsion due to eccentricity tides in explaining the near-resonant systems.

Thus, resonant repulsion driven solely by eccentricity tides cannot fully account for the observed orbital architecture of near-resonant planetary systems. This compels us to explore alternative mechanisms for moving planetary systems away from MMRs. Recently, S. Millholland & G. Laughlin (2019) proposed obliquity tides as a more efficient source of tidal dissipation. They argued that resonant planets are more likely to be locked into a high-obliquity Cassini state due to disk migration and the resulting changes in secular frequencies. In a high-obliquity configuration, the tidal bulge continues to shift within the planet's frame, allowing for efficient dissipation of orbital energy even at low orbital eccentricities. As a result, resonant repulsion driven by obliquity tides appears more plausible than that driven by eccentricity tides alone. Notably, the observed orbital architecture of Kepler-221 is most consistent with rapid evolution under obliquity tides (M. Goldberg & K. Batygin 2021). For a broader population-level analysis of obliquity tides, see E. Louden et al. (2023).

Turbulence in protoplanetary disks may induce stochastic forcing during Type I migration (H. Rein 2012; M. Goldberg & K. Batygin 2023; Y. Wu et al. 2024a). This stochastic forcing tends to broaden the distribution of $\Delta$. However, it remains unclear whether turbulent migration models can reproduce the well-known asymmetric distribution of $\Delta$: a trough of planets with $\Delta$ just below 0 and a pileup of planets with positive 1%–2% deviation (D. C. Fabrycky et al. 2014).

During the final stages of protoplanetary disk evolution, the inner disk edge may undergo outward expansion (B. Liu et al. 2017; B. M. S. Hansen et al. 2024). The asymmetric profile at the disk edge generates diverging torques on neighboring planets. B. Liu et al. (2017) and B. M. S. Hansen et al. (2024) proposed that these torques could pull initially resonant planets out of resonance. Similarly, C. W. Ormel et al. (2017) suggested that this mechanism might explain the architecture of the TRAPPIST-1 system, specifically by removing the inner two planets from first-order MMR while maintaining their three-body Laplace resonance. However, the extent to which this mechanism affects resonant planets located far from the disk's inner edge remains to be explored.

The cumulative effect of scattering by planetesimals may also account for the observed distributions of $\Delta$ and the nonzero free eccentricity (S. Chatterjee & E. B. Ford 2015; S. N. Raymond et al. 2022; Y. Wu et al. 2024b). To produce the observed 1%–2% $\Delta$, the total mass of scattered planetesimals typically needs to be a few percent of the planet's mass. S. N. Raymond et al. (2022) cautioned that resonant-chain systems are so delicate that this amount of planetesimal scattering could destabilize the entire system. R. Li et al. (2024) argued that orbital instability might play a significant role in shaping the observed orbital architecture of near-resonant planets. Contrary to conventional wisdom, R. Li et al. (2024) showed that merger events do not entirely eliminate near-resonant pairs in a planetary system. Instead, planets that were not involved in mergers tend to accumulate at period ratios slightly wider than resonance.

J. Lin et al. (2024) recently proposed that divergent encounters between near-resonant planets tend to push them wider of resonance while generating significant orbital eccentricities. However, orchestrating such encounters for all planets in a resonant chain presents a significant challenge, especially without inducing orbital instability.

As discussed above, a variety of alternative theories have been proposed to explain the observed orbital architecture of near-resonant planets. These include orbital instability (R. Li et al. 2024), disk turbulence (M. Goldberg & K. Batygin 2023), disk edge expansion (B. Liu et al. 2017; B. M. S. Hansen et al. 2024), obliquity tides (S. Millholland & G. Laughlin 2019; E. Louden et al. 2023), planetesimal scatterings (S. Chatterjee & E. B. Ford 2015; Y. Wu et al. 2024b), and divergent encounters (J. Lin et al. 2024). Our failed attempt to attribute the observed architecture solely to resonant repulsion driven by eccentricity tides suggests that one or more of these alternative mechanisms must play a significant role. More careful investigations are required to constrain the relative contributions of the alternative dynamical processes.

### 4.2. Caveats and Future Work

We now list some shortcomings of our work and suggest potential avenues for future studies:

1. *Initial condition.* In this work we assumed that all planet pairs begin with MMR. However, it remains to be tested whether young planetary systems ($\sim$10 Myr old) that have recently completed planet formation are still in MMR or have already been dislodged. If mechanisms such as disk turbulence (M. Goldberg & K. Batygin 2023) and disk edge expansion (B. Liu et al. 2017; B. M. S. Hansen et al. 2024) are primarily responsible for removing systems from MMR, $\sim$10 Myr old systems should already be dislodged. Conversely, other mechanisms such as orbital instability (R. Li et al. 2024), obliquity tides (S. Millholland & G. Laughlin 2019; E. Louden et al. 2023), and planetesimal scatterings (S. Chatterjee & E. B. Ford 2015; Y. Wu et al. 2024b) may require tens to hundreds of Myr to manifest. The discovery and detailed characterization of planetary systems younger than $\sim$10 Myr old will be instrumental in resolving this question.
2. *Self-consistent radius evolution.* Our exploration of radius inflation did not account for the interplay between resonant repulsion and radius evolution. It is plausible that tidal dissipation may sustain an inflated planetary radius for an extended period. Observational evidence seems to support this hypothesis. For example, GJ 436 b (C. V. Morley et al. 2017) and WASP-107 b (D. K. Sing et al. 2024; L. Welbanks et al. 2024; H. Yu & F. Dai 2024) both have inflated planetary radii that are attributable to eccentricity tides. Furthermore, it has been noted that near-resonant planets are generally puffier than their nonresonant counterparts (S. Millholland 2019; A. Leleu et al. 2024). Future studies should explore models that couple resonant repulsion with the evolution of planetary radius.
3. *Direct N-body simulations.* In this work, we modeled resonant repulsion using Equation (1), which is strictly valid for isolated pairs of near-resonant planets. A more accurate approach would involve full $N$-body simulations with eccentricity tides, such as those implemented in REBOUNDX (D. Tamayo et al. 2020). A comprehensive suite of $N$-body simulations could simultaneously account for dynamical instabilities and other processes, which may all play a role in shaping the final orbital architecture.
4. *Higher-order resonances.* Our paper exclusively focused on first-order MMRs, as traditional resonant repulsion theory was derived for these resonances (Y. Lithwick & Y. Wu 2012; K. Batygin & A. Morbidelli 2013). Higher-order MMRs are not expected to show a positive deviation in period ratio $\Delta$ under tidal dissipation (N. Bailey et al. 2022). However, the $\Delta$ distribution near a higher-order resonance still encodes valuable information about the dynamical evolution of planetary systems and warrants further investigation.

## 5. Conclusion

Resonant repulsion coupled with eccentricity tides was among the first explanations proposed for the positive deviation in period ratio $\Delta$ observed in planet pairs near first-order MMRs (J. C. B. Papaloizou & C. Terquem 2010; Y. Lithwick & Y. Wu 2012; K. Batygin & A. Morbidelli 2013). However, the required tidal dissipation rate is often unphysically small,

$Q_p' \lesssim 10$ for some observed near-resonant systems. In this study, we explored three potential effects that could reduce the required tidal dissipation rate or, equivalently, increase $Q_p'$.

We found that incorporating radius inflation could raise the required tidal quality factor by approximately half an order of magnitude. Including additional, undetected planets closer to the host star could further increase $Q_p'$ by almost an order of magnitude. Finally, the initial deviation in period ratio $\Delta_i$ from disk migration simulations is so small, $\log_{10}(\Delta_i) = -3.4 \pm 0.5$, that they have a negligible impact on $Q_p'$.

When combining all three effects, the tidal quality factor increases to $\log_{10}(Q_p') = 1.2 \pm 2.1$ for the super-Earths and terrestrial-sized planets, and $\log_{10}(Q_p') = 2.4 \pm 1.7$ for mini-Neptunes ($>2\ R_\oplus$). Despite these improvements, these values remain inconsistent with solar system estimates of $\log_{10}(Q_p') = 3$ and 5 for rocky and gaseous planets.

Thus, eccentricity tides alone cannot fully explain the observed $\Delta$ distribution as well as the nonzero TTV phases. Other mechanisms, such as obliquity tides, planetesimal scattering, expanding disk inner edges, disk turbulence, divergent encounters, and dynamical instabilities, are likely important in shaping planetary systems near first-order MMRs.

## Appendix

Table 1 summarizes the characteristics of sample near-resonance systems, including uncertainties in $\log_{10} Q_p^{'}$ and planetary counts, as discussed in the main text.

**Table 1**
Characteristics of the Sample near Resonance

| $\log_{10} Q_p'$ | $N_P$ | $\Delta_{obs}$ | $P_{obs}$ (days) | Radius of Planet ($R_\oplus$) | Planet Name (Inner Planet of a Pair) | Planet Mass ($M_\oplus$) | Age from T. A. Berger et al. (2020) (Gyr) |
|---|---|---|---|---|---|---|---|
| $-2.9 \pm 0.43$ | 1 | 0.023 | 6.8 | 0.76 | Kepler-431 b | 0.41 | 5.6 |
| $-1.2 \pm 0.63$ | 1 | 0.010 | 3.6 | 0.40 | Kepler-444 b | 0.045 | 6.1 |
| $-1.1 \pm 0.60$ | 1 | 0.025 | 2.9 | 0.65 | Kepler-1542 c | 0.23 | 12 |
| $-1.0 \pm 0.60$ | 3 | 0.023 | 28 | 1.9 | Kepler-341 d | 4.8 | 11 |
| $-0.85 \pm 0.48$ | 1 | 0.026 | 7.5 | 0.84 | Kepler-450 d | 0.56 | 4.6 |
| $-0.53 \pm 0.48$ | 1 | 0.013 | 7.4 | 0.74 | Kepler-345 b | 0.36 | 9.6 |
| $-0.033 \pm 0.63$ | 1 | 0.028 | 5.2 | 1.2 | Kepler-341 b | 1.9 | 6.4 |
| $0.075 \pm 0.73$ | 1 | 0.013 | 15 | 1.4 | Kepler-128 b | 3.8 | 9.7 |
| $0.24 \pm 0.54$ | 1 | 0.020 | 7.7 | 2.7 | Kepler-880 b | 6.7 | 9.6 |
| $0.24 \pm 0.71$ | 1 | 0.023 | 12 | 1.4 | Kepler-386 b | 3.5 | 9.2 |
| $0.28 \pm 0.52$ | 2 | 0.026 | 9.8 | 2.0 | Kepler-244 c | 5.2 | 11 |
| $0.30 \pm 0.57$ | 1 | 0.022 | 8.5 | 1.8 | Kepler-331 b | 4.7 | 11 |
| $0.31 \pm 0.49$ | 1 | 0.023 | 6.5 | 1.0 | Kepler-192 d | 1.1 | 4.8 |
| $0.31 \pm 0.73$ | 1 | 0.0034 | 23 | 1.1 | Kepler-384 b | 1.6 | 0.36 |
| $0.40 \pm 0.53$ | 1 | 0.022 | 2.5 | 1.1 | Kepler-327 b | 1.5 | 5.2 |
| $0.56 \pm 0.60$ | 1 | 0.0100 | 12 | 1.1 | Kepler-59 b | 1.5 | 2.3 |
| $0.61 \pm 0.68$ | 1 | 0.021 | 12 | 1.0 | Kepler-595 c | 3.3 | 8.4 |
| $0.66 \pm 0.55$ | 2 | 0.0073 | 7.0 | 1.1 | Kepler-339 c | 1.7 | 4.6 |
| $0.75 \pm 0.74$ | 1 | 0.018 | 14 | 1.4 | Kepler-127 b | 3.6 | 3.1 |
| $0.89 \pm 0.56$ | 2 | 0.021 | 3.3 | 1.1 | Kepler-374 c | 1.5 | 2.1 |
| $0.92 \pm 0.75$ | 1 | 0.025 | 15 | 2.5 | Kepler-340 b | 6.4 | 3.2 |
| $0.96 \pm 0.56$ | 2 | 0.010 | 8.0 | 1.6 | Kepler-394 b | 4.2 | 5.5 |
| $1.2 \pm 0.49$ | 1 | 0.0031 | 5.3 | 0.46 | Kepler-102 b | 1.1 | 11 |
| $1.2 \pm 0.86$ | 2 | 0.0099 | 10 | 1.2 | Kepler-197 c | 2.2 | 0.39 |
| $1.2 \pm 0.70$ | 3 | 0.0027 | 26 | 2.0 | Kepler-342 c | 5.0 | 6.8 |
| $1.3 \pm 0.46$ | 1 | 0.023 | 5.7 | 2.1 | Kepler-183 b | 5.3 | 8.2 |
| $1.3 \pm 0.51$ | 2 | 0.011 | 6.2 | 1.2 | Kepler-169 c | 2.1 | 9.0 |
| $1.5 \pm 0.62$ | 1 | 0.028 | 29 | 3.9 | Kepler-30 b | 11 | 0.28 |
| $1.5 \pm 0.67$ | 1 | 0.011 | 10 | 1.8 | Kepler-11 b | 1.9 | 4.6 |
| $1.6 \pm 0.77$ | 1 | 0.016 | 13 | 3.5 | Kepler-79 b | 11 | 8.0 |
| $1.6 \pm 0.61$ | 1 | 0.013 | 6.3 | 2.1 | Kepler-120 b | 5.5 | 3.4 |
| $1.7 \pm 0.63$ | 1 | 0.028 | 3.2 | 1.5 | Kepler-107 b | 3.8 | 5.5 |
| $1.8 \pm 0.55$ | 1 | 0.0012 | 7.5 | 0.80 | Kepler-1972 b | 2.0 | 1.7 |
| $1.9 \pm 0.60$ | 1 | 0.025 | 3.4 | 2.0 | Kepler-267 b | 5.1 | 0.86 |
| $1.9 \pm 0.63$ | 1 | 0.028 | 3.1 | 1.3 | Kepler-181 b | 2.5 | 5.3 |
| $1.9 \pm 0.63$ | 1 | 0.022 | 21 | 5.5 | Kepler-31 b | 13 | 1.9 |
| $2.0 \pm 0.53$ | 1 | 0.017 | 5.3 | 2.5 | Kepler-269 b | 6.2 | 5.5 |
| $2.1 \pm 0.47$ | 1 | 0.020 | 6.2 | 2.7 | Kepler-25 b | 8.7 | 3.2 |
| $2.1 \pm 0.62$ | 1 | 0.018 | 3.9 | 1.6 | Kepler-226 b | 4.0 | 12 |
| $2.1 \pm 0.52$ | 2 | 0.0098 | 8.1 | 2.3 | Kepler-24 b | 11 | 3.3 |
| $2.2 \pm 0.60$ | 1 | 0.028 | 10 | 2.5 | Kepler-29 b | 5.0 | 10.0 |
| $2.2 \pm 0.49$ | 1 | 0.0048 | 8.3 | 1.8 | Kepler-85 b | 1.8 | 7.0 |
| $2.4 \pm 0.65$ | 1 | 0.019 | 3.0 | 1.4 | Kepler-272 b | 3.9 | 8.7 |
| $2.4 \pm 0.49$ | 1 | 0.0085 | 7.1 | 1.6 | Kepler-23 b | 2.6 | 3.2 |
| $2.4 \pm 0.40$ | 2 | 0.028 | 9.8 | 2.8 | Kepler-83 b | 7.1 | 8.6 |
| $2.4 \pm 0.69$ | 2 | 0.0069 | 12 | 2.1 | Kepler-254 c | 5.5 | 4.3 |

**Table 1**
(Continued)

| $\log_{10} Q'_p$ | $N_P$ | $\Delta_{obs}$ | $P_{obs}$ (days) | Radius of Planet ($R_\oplus$) | Planet Name (Inner Planet of a Pair) | Planet Mass ($M_\oplus$) | Age from T. A. Berger et al. (2020) (Gyr) |
|---|---|---|---|---|---|---|---|
| 2.4 ± 0.80 | 2 | 0.0091 | 13 | 2.6 | Kepler-176 c | 6.5 | 5.8 |
| 2.4 ± 0.72 | 1 | 0.027 | 2.6 | 1.6 | Kepler-1530 b | 4.3 | 3.0 |
| 2.6 ± 0.72 | 1 | 0.019 | 2.2 | 1.5 | Kepler-326 b | 4.0 | 5.3 |
| 2.7 ± 0.53 | 1 | 0.014 | 4.0 | 1.2 | Kepler-402 b | 2.2 | 8.9 |
| 2.7 ± 0.55 | 1 | 0.014 | 5.9 | 2.0 | Kepler-28 b | 1.6 | 4.4 |
| 2.8 ± 0.76 | 1 | 0.018 | 2.8 | 1.7 | Kepler-221 b | 4.4 | 4.9 |
| 2.9 ± 0.68 | 1 | 0.0016 | 21 | 1.2 | KOI-3503 b | 9.2 | 3.7 |
| 3.1 ± 0.58 | 1 | 0.014 | 5.7 | 3.1 | Kepler-57 b | 25 | 1.8 |
| 3.2 ± 0.64 | 4 | 0.0055 | 28 | 2.4 | Kepler-55 b | 6.1 | 1.7 |
| 3.3 ± 0.61 | 2 | 0.0095 | 5.7 | 1.7 | Kepler-968 c | 4.4 | 1.1 |
| 3.3 ± 0.77 | 2 | 0.016 | 10 | 2.8 | Kepler-58 b | 36 | 4.5 |
| 3.4 ± 0.66 | 1 | 0.012 | 4.8 | 1.9 | Kepler-48 b | 3.9 | 11 |
| 3.6 ± 0.67 | 1 | 0.0065 | 10 | 2.7 | Kepler-385 b | 6.8 | 3.5 |
| 3.6 ± 0.70 | 1 | 0.019 | 11 | 6.5 | Kepler-56 b | 22 | 1.6 |
| 3.7 ± 0.67 | 1 | 0.0036 | 10 | 2.4 | Kepler-307 b | 7.4 | 5.7 |
| 3.8 ± 0.60 | 1 | 0.015 | 2.4 | 1.6 | Kepler-1065 c | 4.2 | 5.9 |
| 3.8 ± 0.73 | 1 | 0.0014 | 14 | 1.9 | KOI-1599.02 | 9.0 | 11 |
| 4.0 ± 0.79 | 2 | 0.022 | 15 | 4.0 | Kepler-27 b | 9.8 | 8.4 |
| 4.1 ± 0.55 | 1 | 0.027 | 3.1 | 1.6 | Kepler-416 d | 4.2 | 3.8 |
| 4.3 ± 0.62 | 2 | 0.0079 | 3.1 | 1.5 | Kepler-80 d | 6.8 | 10 |
| 4.3 ± 0.56 | 2 | 0.010 | 7.2 | 2.6 | Kepler-49 b | 9.8 | 1.2 |
| 4.3 ± 0.54 | 1 | 0.011 | 6.0 | 2.4 | Kepler-81 b | 6.1 | 9.3 |
| 4.3 ± 0.58 | 2 | 0.019 | 2.9 | 1.5 | Kepler-32 e | 4.6 | 3.8 |
| 4.5 ± 0.56 | 2 | 0.013 | 19 | 8.3 | Kepler-9 b | 43 | 3.1 |
| 4.6 ± 0.84 | 1 | 0.0022 | 10 | 0.64 | Kepler-138 b | 0.070 | 0.34 |
| 4.8 ± 0.44 | 1 | 0.0046 | 8.0 | 2.1 | Kepler-54 b | 5.4 | 6.7 |
| 5.0 ± 0.66 | 2 | 0.0056 | 4.7 | 1.2 | Kepler-1669 d | 2.2 | 7.9 |
| 5.1 ± 0.60 | 2 | 0.0074 | 5.5 | 3.6 | Kepler-305 b | 10 | 6.0 |
| 5.2 ± 0.59 | 2 | 0.00040 | 20 | 2.1 | Kepler-372 c | 5.3 | 2.2 |
| 6.5 ± 0.43 | 1 | 0.00022 | 7.1 | 1.7 | Kepler-60 b | 4.2 | 5.4 |
| 6.6 ± 0.62 | 1 | 0.00015 | 7.8 | 1.7 | Kepler-50 b | 4.4 | 7.6 |
| 6.7 ± 0.50 | 2 | 0.024 | 1.2 | 0.78 | Kepler-42 b | 0.44 | 3.4 |

**Note.** The uncertainty in $\log_{10} Q'_p$ represents the standard deviation of $Q'_p$ values derived from randomly selected parameters (after three effects), as detailed in the main text. $N_P$ denotes the number of planets in the system. $P_{obs}$ is the period of the inner planet within the pair. The standard deviation of age from T. A. Berger et al. (2020) is 3.9.

## ORCID iDs

Fei Dai https://orcid.org/0000-0002-8958-0683

## References

Bailey, N., Gilbert, G., & Fabrycky, D. 2022, AJ, 163, 13
Barber, M. G., Thao, P. C., Mann, A. W., et al. 2024, ApJL, 973, L30
Batygin, K., Adams, F. C., & Becker, J. 2023, ApJL, 951, L19
Batygin, K., & Morbidelli, A. 2013, AJ, 145, 1
Berger, T. A., Huber, D., Gaidos, E., van Saders, J. L., & Weiss, L. M. 2020, AJ, 160, 108
Borucki, W. J., Koch, D. G., Basri, G., et al. 2011, ApJ, 728, 117
Brasser, R., Pichierri, G., Dobos, V., & Barr, A. C. 2022, MNRAS, 515, 2373
Chatterjee, S., & Ford, E. B. 2015, ApJ, 803, 33
Chen, H., & Rogers, L. A. 2016, ApJ, 831, 180
Choksi, N., & Chiang, E. 2020, MNRAS, 495, 4192
Choksi, N., & Chiang, E. 2023, MNRAS, 522, 1914
Crossfield, I. J. M., Malik, M., Hill, M. L., et al. 2022, ApJL, 937, L17
Dai, F., Goldberg, M., Batygin, K., et al. 2024, AJ, 168, 239
Dai, F., Masuda, K., Beard, C., et al. 2023, AJ, 165, 33
Dai, F., Masuda, K., & Winn, J. N. 2018, ApJL, 864, L38
Dai, F., Masuda, K., Winn, J. N., & Zeng, L. 2019, ApJ, 883, 79
David, T. J., Petigura, E. A., Luger, R., et al. 2019, ApJL, 885, L12
Delisle, J. B., & Laskar, J. 2014, A&A, 570, L7
Dressing, C. D., Charbonneau, D., Dumusque, X., et al. 2015, ApJ, 800, 135
Emsenhuber, A., Mordasini, C., Burn, R., et al. 2021, A&A, 656, A69
Fabrycky, D. C., Lissauer, J. J., Ragozzine, D., et al. 2014, ApJ, 790, 146
Fang, J., & Margot, J.-L. 2012, ApJ, 761, 92
Ford, E. B., Fabrycky, D. C., Steffen, J. H., et al. 2012, ApJ, 750, 113
Fortney, J. J., Marley, M. S., & Barnes, J. W. 2007, ApJ, 659, 1661
Fulton, B. J., Petigura, E. A., Howard, A. W., et al. 2017, AJ, 154, 109
Ginzburg, S., Schlichting, H. E., & Sari, R. 2018, MNRAS, 476, 759
Goldberg, M., & Batygin, K. 2021, AJ, 162, 16
Goldberg, M., & Batygin, K. 2023, ApJ, 948, 12
Goldberg, M., Batygin, K., & Morbidelli, A. 2022, Icar, 388, 115206
Goldreich, P., & Soter, S. 1966, Icar, 5, 375
Goldreich, P., & Tremaine, S. 1979, ApJ, 233, 857
Hadden, S., & Lithwick, Y. 2014, ApJ, 787, 80
Hadden, S., & Lithwick, Y. 2017, AJ, 154, 5
Hamer, J. H., & Schlaufman, K. C. 2024, AJ, 167, 55
Hansen, B. M. S., Yu, T.-Y., & Hasegawa, Y. 2024, OJAp, 7, 61
Hu, R., Bello-Arufe, A., Zhang, M., et al. 2024, Natur, 630, 609
Huang, S., & Ormel, C. W. 2022, MNRAS, 511, 3814
Izidoro, A., Ogihara, M., Raymond, S. N., et al. 2017, MNRAS, 470, 1750
Kreidberg, L., Koll, D. D. B., Morley, C., et al. 2019, Natur, 573, 87
Lee, E. J. 2019, ApJ, 878, 36
Lee, M. H., Fabrycky, D., & Lin, D. N. C. 2013, ApJ, 774, 52
Leleu, A., Delisle, J.-B., Burn, R., et al. 2024, A&A, 687, L1
Li, R., Chiang, E., Choksi, N., & Dai, F. 2024, arXiv:2408.10206
Lin, D. N. C., & Papaloizou, J. 1986, ApJ, 309, 846
Lin, J., Dudiak, I., Hadden, S., & Tamayo, D. 2024, arXiv:2412.12415
Lithwick, Y., & Wu, Y. 2011, ApJ, 739, 31

Lithwick, Y., & Wu, Y. 2012, ApJL, 756, L11
Lithwick, Y., Xie, J., & Wu, Y. 2012, ApJ, 761, 122
Liu, B., Ormel, C. W., & Lin, D. N. C. 2017, A&A, 601, A15
Livingston, J. H., Crossfield, I. J. M., Petigura, E. A., et al. 2018, AJ, 156, 277
Louden, E., Laughlin, G., & Millholland, S. 2023, ApJL, 958, L21
Luque, R., Osborn, H. P., Leleu, A., et al. 2023, Natur, 623, 932
MacDonald, M. G., Ragozzine, D., Fabrycky, D. C., et al. 2016, AJ, 152, 105
Mann, A. W., Wood, M. L., Schmidt, S. P., et al. 2022, AJ, 163, 156
Masset, F. S., Morbidelli, A., Crida, A., & Ferreira, J. 2006, ApJ, 642, 478
Matsumoto, Y., & Ogihara, M. 2020, ApJ, 893, 43
McNeil, D., Duncan, M., & Levison, H. F. 2005, AJ, 130, 2884
Millholland, S. 2019, ApJ, 886, 72
Millholland, S., & Laughlin, G. 2019, NatAs, 3, 424
Mills, S. M., Fabrycky, D. C., Migaszewski, C., et al. 2016, Natur, 533, 509
Morley, C. V., Knutson, H., Line, M., et al. 2017, AJ, 153, 86
Murray, C. D., & Dermott, S. F. 1999, Solar System Dynamics (Cambridge: Cambridge Univ. Press)
NASA Exoplanet Science Institute 2020, Planetary Systems Table, NASA IPAC
Nelson, R. P. 2018, in Handbook of Exoplanets, ed. H. J. Deeg & J. A. Belmonte (Berlin: Springer), 139
Ogihara, M., Kokubo, E., Suzuki, T. K., & Morbidelli, A. 2018, A&A, 615, A63
Ormel, C. W., Liu, B., & Schoonenberg, D. 2017, A&A, 604, A1
Otegi, J. F., Bouchy, F., & Helled, R. 2020, A&A, 634, A43
Owen, J. E., & Wu, Y. 2017, ApJ, 847, 29
Papaloizou, J. C. B., Szuszkiewicz, E., & Terquem, C. 2017, MNRAS, 476, 5032
Papaloizou, J. C. B., & Terquem, C. 2010, MNRAS, 405, 573
Paxton, B., Marchant, P., Schwab, J., et al. 2015, ApJS, 220, 15
Peale, S. J. 1976, ARA&A, 14, 215
Petrovich, C., Deibert, E., & Wu, Y. 2019, AJ, 157, 180
Pichierri, G., & Morbidelli, A. 2020, MNRAS, 494, 4950
Pichierri, G., Morbidelli, A., & Crida, A. 2018, CeMDA, 130, 54
Plavchan, P., Barclay, T., Gagné, J., et al. 2020, Natur, 582, 497
Pu, B., & Lai, D. 2019, MNRAS, 488, 3568
Raymond, S. N., Izidoro, A., Bolmont, E., et al. 2022, NatAs, 6, 80
Rebull, L. M., Stauffer, J. R., Cody, A. M., et al. 2018, AJ, 155, 196
Rein, H. 2012, MNRAS, 427, L21
Ricker, G. R., Winn, J. N., Vanderspek, R., et al. 2014, Proc. SPIE, 9143, 914320
Rodriguez, J. E., Becker, J. C., Eastman, J. D., et al. 2018, AJ, 156, 245
Rogers, L. A. 2015, ApJ, 801, 41
Rowe, J. F., Bryson, S. T., Marcy, G. W., et al. 2014, ApJ, 784, 45
Schlaufman, K. C. 2010, ApJ, 719, 602
Shapiro, S. L., & Teukolsky, S. A. 1986, Black Holes, White Dwarfs and Neutron Stars: The Physics of Compact Objects (New York: Wiley)
Silburt, A., & Rein, H. 2015, MNRAS, 453, 4089
Sing, D. K., Rustamkulov, Z., Thorngren, D. P., et al. 2024, Natur, 630, 831
Spalding, C., & Batygin, K. 2016, ApJ, 830, 5
Tamayo, D., Rein, H., Shi, P., & Hernandez, D. M. 2020, MNRAS, 491, 2885
Terquem, C., & Papaloizou, J. C. B. 2007, ApJ, 654, 1110
Terquem, C., & Papaloizou, J. C. B. 2019, MNRAS, 482, 530
Tittemore, W. C., & Wisdom, J. 1990, Icar, 85, 394
Vach, S., Zhou, G., Huang, C. X., et al. 2024, AJ, 167, 210
Wang, S., & Lin, D. N. C. 2023, AJ, 165, 174
Ward, W. R. 1997, Icar, 126, 261
Welbanks, L., Bell, T. J., Beatty, T. G., et al. 2024, Natur, 630, 836
Wittrock, J. M., Plavchan, P. P., Cale, B. L., et al. 2023, AJ, 166, 232
Wong, K. H., & Lee, M. H. 2024, AJ, 167, 112
Wood, M. L., Mann, A. W., Barber, M. G., et al. 2023, AJ, 165, 85
Wu, Y. 2005, ApJ, 635, 688
Wu, Y., Chen, Y.-X., & Lin, D. N. C. 2024a, MNRAS, 528, L127
Wu, Y., Malhotra, R., & Lithwick, Y. 2024b, ApJ, 971, 5
Yoder, C. F. 1995, in Global Earth Physics: A Handbook of Physical Constants, ed. T. J. Ahrens (Washington, D. C.: American Geophysical Union), 1
Yu, H., & Dai, F. 2024, ApJ, 972, 159
Zhang, M., Hu, R., Inglis, J., et al. 2024, ApJL, 961, L44